Hyperbranched polyurethane/Fe_3O_4 nanoparticles decorated multiwalled carbon nanotube thermosetting nanocomposites as microwave actuated shape memory materials

Hemjyoti Kalita and Niranjan Karak[a)]
Advanced Polymer & Nanomaterial Laboratory, Department of Chemical Sciences, Tezpur University, Tezpur 784028, Assam, India

(Received 10 May 2013; accepted 3 July 2013)

Hyperbranched polyurethane/Fe_3O_4 nanoparticles decorated multiwalled carbon nanotube (Fe_3O_4-MWCNT) nanocomposites were prepared by the in situ polymerization technique. The presence of Fe_3O_4 nanoparticles on the surface of the MWCNTs was confirmed by x-ray diffraction and transmission electron microscopic studies. The saturation magnetization value of Fe_3O_4-MWCNT was 0.23 emu/g. The glycidyl ether of bisphenol-A epoxy cured thermosetting nanocomposites exhibited enhanced tensile strength (6.4–38.5 MPa), scratch hardness (3.0–8.5 kg), and thermal stability (241–292 °C) with the increase of loading of Fe_3O_4-MWCNT (0–2 wt%). The nanocomposites possess good shape fixity over the repeated cycles of test. The nanocomposites also showed good shape recovery under the application of microwave irradiation. The shape recovery speed was found to be increased with the increase of the content of Fe_3O_4-MWCNT. Thus, the studied thermosetting nanocomposites have potential to be used as noncontact shape memory materials.

I. INTRODUCTION

Shape memory polymer is a stimuli-responsive material that can be deformed from a permanent shape to a fixed temporary shape by cooling it below the transition temperature (T_{trans}) and reverts back to the original shape under the application of stimulus such as heat, light, water, electric field, and magnetic field.[1–5] Shape memory polymers (SMPs) have attracted great attention over the shape memory alloys due to the advantages such as easy processing, lightweight characteristic, low cost, large recoverable strain, and low toxicity.[6,7] However, SMPs have some demerits that impose great challenges to their broad applications, such as poor mechanical properties, slow recovery speed, and short life cycle.[8,9] Such limitations have motivated the scientists and technologists to develop new desired SMPs. Among different SMPs, segmented polyurethanes with appropriate hard and soft domains exhibited attractive shape memory behaviors. Further design of such polyurethane with novel molecular architecture like hyperbranched structure offers added advantages such as low viscosity, high solubility, high reactivity, and good compatibility with other materials including polymers. In addition to above utilization of bio-based renewable resources like vegetable oils, adding new feathers into them as such bio-based hyperbranched polyurethanes are very interesting in the current scenario of advanced polymeric materials for today's society. However, to overcome the drawbacks of such virgin hyperbranched polyurethanes, formation of suitable nanocomposites with appropriate nanomaterials such as carbon nanotube (CNT), carbon nanofiber, glass fiber, nanohybrid material, etc. is an attractive choice in this case too. These nanocomposites are expected to be the most versatile materials that can overcome the above limitations of SMPs.[10,11] Furthermore, these limitations may also be addressed by cross-linking the SMP with the other suitable polymers as cross-linking can modify the mechanical properties and shape memory behavior because of change of nature and numbers of net points in the matrix.[12] Glycidyl ether epoxy of bisphenol-A resin was used here as a cross-linking agent due to the advantages such as excellent weather resistance, good flowability (450–650 MPa at 25 °C), low shrinkage on curing (<0.01%), good thermal (200–220 °C), and dielectric behavior (dielectric constant is 4–5) along with good compatibility with the polyurethane.[13,14]

Again, among different nanomaterials, CNTs are one-dimensional structures that possess excellent mechanical properties, high thermal and electrical conductivity (6600 W/mK and 10^4 S/cm).[15–17] These fascinating properties and their wide potential applications encourage to utilizing them as nanomaterials in polymer nanocomposites. However, the preparation of CNT-based nanocomposites is very difficult because of their strong tendency of agglomeration.[18–20] Various methods have been explored to enhance the dispersion of CNT in the polymer matrix through

a)Address all correspondence to this author.
e-mail: karakniranjan@yahoo.com
DOI: 10.1557/jmr.2013.213

 © Materials Research Society 2013

https://doi.org/10.1557/jmr.2013.213 Published online by Cambridge University Press

covalent and physical linkages. However, CNTs decorated with other inorganic nanomaterials such as ZnO, Fe_3O_4, Cu, etc. have gained increasing attention due to increasing dispersion as well as modification of intrinsic properties of the CNT, and thus find potential applications in different fields.[21–25] Further, it is also reported that Fe_3O_4 and multiwalled carbon nanotubes (MWCNTs) have microwave absorption characteristics.[26,27] In the current study, a nanohybrid system was, therefore, prepared by decorating the MWCNTs with the Fe_3O_4 nanoparticles.

Furthermore, the SMP triggering with direct heating is not suitable for the biomedical applications. In the present study, microwave energy was used as a noncontact stimulus to investigate the shape memory behaviors. Microwave is an electromagnetic wave in the range of 300 MHz to 300 GHz that corresponds to wave lengths of 1 m to 1 mm. The absorbed microwave energy is transferred into thermal energy through molecular friction and collisions. Once this induced temperature activated the polymer chains, the shape memory effect is observed.

In the present study, therefore, Fe_3O_4 nanoparticles decorated multiwalled carbon nanotube (Fe_3O_4-MWCNT) nanohybrid/hyperbranched polyurethane (HBPU) thermosetting nanocomposites were prepared to investigate the performance including shape memory behaviors.

II. EXPERIMENTAL

A. Materials

Glycerol (99%, Merck, Mumbai, India), poly(ε-caprolactone)diol (PCL, Solvay Co., Warrington, UK; M_n = 3000 g/mol), 1,4-butanediol (99%, Merck, Germany), and triethanolamine (99%, TEA; Merck, India) were used after drying in a vacuum oven at 60 °C for 12 h. *Mesua ferrea* L. seeds were collected from Darang, Assam, India. The oil was isolated by the solvent soaking method and purified by the alkali refining technique. Monoglyceride of the oil was prepared by the standard procedure.[28] Nitric acid (Merck, India), sulfuric acid (Merck, India), iron (III) chloride hexahydrate ($FeCl_3{\cdot}6H_2O$) (Merck, India), iron (II) chloride tetrahydrate ($FeCl_2{\cdot}4H_2O$) (Merck, Germany), ammonia solution (30 vol/vol%, Qualigens Fine Chemicals Ltd., Mumbai, India), Calcium oxide (S.D. Fine Chemical Ltd., Mumbai, India), and toluene diisocyanate (80% of 2,4 and 20% of 2,6 isomers, TDI; Sigma Aldrich, Munich, Germany) were used as received. Xylene (99%, Merck, India) and dimethylformamide (DMF, 99%; Merck, India) were vacuum distilled and kept in 4A type molecular sieves before use. MWCNTs with a diameter and length of about 10–20 nm and 20 μm, respectively, were purchased from Iiljin Nanotech, Korea. The epoxy resin, a glycidyl bisphenol-A based epoxy (product of epichlorohydrin and bisphenol-A) with an epoxy equivalent of 182–192 g/equivalent (Ciba Geigy, Mumbai, India), was used as supplied.

B. Preparation and characterization techniques

1. Preparation of Fe_3O_4-MWCNT nanohybrid

The pristine MWCNTs were first treated by a 3:1 (vol/vol) mixture of concentrated H_2SO_4 and HNO_3 at 90 °C for 1.5 h. After acid treatment, they were washed using distilled water until the pH value reaches 7. Then, the washed MWCNTs were dried in a vacuum oven at 50 °C for 24 h. 0.08 g of acid-treated MWCNTs (a-MWCNTs) was dispersed in 50 mL of distilled water for 20 min by ultra-sonication. Then, $FeCl_2{\cdot}4H_2O$ (0.0007 mol) and $FeCl_3{\cdot}6H_2O$ (0.001 mol) were added to the above dispersed solution and stirred for 1.5 h under the N_2 atmosphere. Ammonia solution (30 vol/vol%) was then added slowly into the dispersed solution until the pH reached values of 10–11 followed by heating at 80 °C for 2 h. The black products were washed with distilled water until the pH values reach 7 followed by drying at 50 °C for 24 h in vacuum. The weight ratio of Fe_3O_4 to MWCNTs in the nanohybrid is 1:1. The calculation is based on the amount of Fe_3O_4 produced in mol from $FeCl_2{\cdot}4H_2O$ (0.0007 mol) and $FeCl_3{\cdot}6H_2O$ (0.001 mol) in the weighted amount (0.08 g) of MWCNTs. The mol of Fe_3O_4 is then converted to weight by multiplying with its molecular weight, and the amount is found to be ~0.08 g. Hence, the weight ratio is 1:1.

2. Preparation of thermosetting HBPU/Fe_3O_4-MWCNT nanocomposites

The hyperbranched polyurethane was prepared by the prepolymerization technique, as described in the earlier paper.[29] Briefly, the predried PCL (2.8 mol) and monoglyceride of *Mesua ferrea* L. seed oil (3.78 mol) were placed in a nitrogen-flushed three-neck round bottom flask with 30 mL of xylene at constant stirring. An exactly required amount of TDI (14.76 mol) was added into the reaction mixture and the reaction was continued for 3 h at 80 °C to obtain the prepolymer. Then 1,4-butanediol (2 mol) and TEA (4.12 mol) were added to the prepolymer at room temperature followed by heating at 80 °C for another 2 h. The precalculated amount of Fe_3O_4-MWCNTs was dispersed in DMF by ultra-sonication for 10 min. Then the dispersed solution was added drop by drop into the above reaction mixture and continued for another 1 h. To obtain the thermosetting polymer, the above-prepared nanocomposite was mixed with 10 wt% of glycidyl bisphenol-A-based epoxy resin (100% solid content) by mechanical stirring followed by 10 min ultrasonication. The polymer solution was cast on the inert substrates followed by vacuum degassing and cured at 120 °C. The cured films were denoted as HBPU0.2, HBPU1, and HBPU2 corresponding to the Fe_3O_4-MWCNT content of 0.2, 1, and 2 wt%, respectively.

3. Characterization techniques

The x-ray diffraction study was carried out at room temperature (approximately 25 °C) by a Rigaku x-ray

https://doi.org/10.1557/jmr.2013.213 Published online by Cambridge University Press

diffractometer (Miniflex, Ipswich, UK) (Cu K_α, wave length: 1.54 A°) over a range of $2\theta = 10–70°$. The infrared spectra of the polyurethanes were recorded by impact 410, Nicolet (Madison, WI) Fourier transform infrared (FTIR) spectrophotometer using KBr pellets. The Raman spectra of MWCNTs were recorded by Invia Renishaw Raman spectrometer, England (argon ion laser with excitation wave length 514.5 nm). Lakeshore vibrating sample magnetometer (VSM; Model 7410) within the range of +20,000 to −20,000 Oe at room temperature was used to study the magnetic behavior of the samples. The thermogravimetric analysis (TGA) was done by a Simadzu, Japan thermal analyzer, TG50, with a nitrogen flow rate of 30 mL/min at the heating rate of 10 °C/min. The differential scanning calorimetry (DSC) was done by DSC 60, Simadzu, Japan, at 3 °C/min heating rate under the nitrogen flow rate of 30 mL/min from −30–150 °C by following heating–cooling–heating cycle. The surface morphology and distribution of the MWCNTs in the nanocomposites were studied using a transmission electron microscope (TEM), JEOL JEM 2100 (Tokyo, Japan), at an operating voltage of 200 kV. The tensile strength and elongation at break were measured with the help of the universal testing machine, Zwick Z010 (Ulm, Germany), with a 10×10^3 N load cell and a crosshead speed of 0.05 m/min using samples of dimensions: $0.1 \times 0.01 \times 0.00035$ m^3. Scratch hardness of the dry film was measured by using a scratch tester, model number 705 (Sheen instrument Ltd., Kingston, UK) with stylus accessory (ASTM D 5178) and a travel speed of 0.03–0.04 m/s. The impact resistance was measured by an impact tester (S.C. Dey & Co., Kolkata, India, 1.0 m is the maximum height) using the standard ASTM D 1037 falling weight method. A weight of 0.85 kg was allowed to fall on the mild steel plate-coated film from minimum to maximum height up to which the film was not damaged. The maximum height was taken as the impact resistance. The swelling was carried out by immersing a weighed amount (W_d) of the cured film in DMF. The samples were removed from the solvent after attaining equilibrium swelling and the weight of the swollen film (W_s) was also measured. The swelling value was calculated by using the following formula:

$$\text{Swelling}\,(\%) = [(W_s - W_d)/W_d] \times 100 \quad . \qquad (1)$$

Strip-like samples of HBPU and nanocomposites with the dimension of $40 \times 2 \times 0.8$ mm^3 were heated at 60 °C (T_m + 20 °C) for 5 min followed by folding into a circular shape. Immediately, the folded samples were quenched to a low temperature [0–5 °C (T_m − 40 °C)] for 5 min to fix the deformed shape. Then, the samples were exposed to the microwave irradiation (Scientific microwave system, Model: CATA 2R, catalyst systems, 2450 MHz, output power: 140–700 W, India) at microwave output power 350 W for the shape recovery study (distance between the source and the sample was 12 cm). The microwave irradiation was maintained during the shape recovery period. The shape recovery and shape fixity are calculated from the following equations:[30]

$$\text{Shape recovery}\,(\%) = [(90 - \theta)/90] \times 100 \quad , \qquad (2)$$

$$\text{Shape fixity}\,(\%) = [\theta/90] \times 100 \quad , \qquad (3)$$

where θ in degree denotes the angle between the tangential line at the midpoint of the sample and the line connecting the midpoint and the end of the curved sample.

III. RESULTS AND DISCUSSION

A. Curing study

From the curing study, it was noticed that the touch free time (minimum time required by the system to resist impression on touching its surface by thumb) at room temperature and the drying time (determined by indenting the cured film by an indenter) at 120 °C decreased with the increase of the loading of Fe_3O_4-MWCNTs in the nanocomposites (Table I). This is due to the increased cross-linking reactions among the –OH/–C=O of Fe_3O_4-MWCNTs, epoxy/hydroxyl groups of the epoxy resin, and free –OH groups of the hyperbranched polyurethane (Scheme 1). Due to the increase of the content of Fe_3O_4-MWCNTs, the number of free –OH and –C=O groups increases in the system; as a result, intercross-linking network formation increased and thereby confers the three-dimensional network structures. The absence of the epoxy band at 916 cm^{-1} after curing in FTIR spectra confirmed the formation of the network structure. The increased cross-linking density of the nanocomposites was also confirmed by the swelling test in DMF.

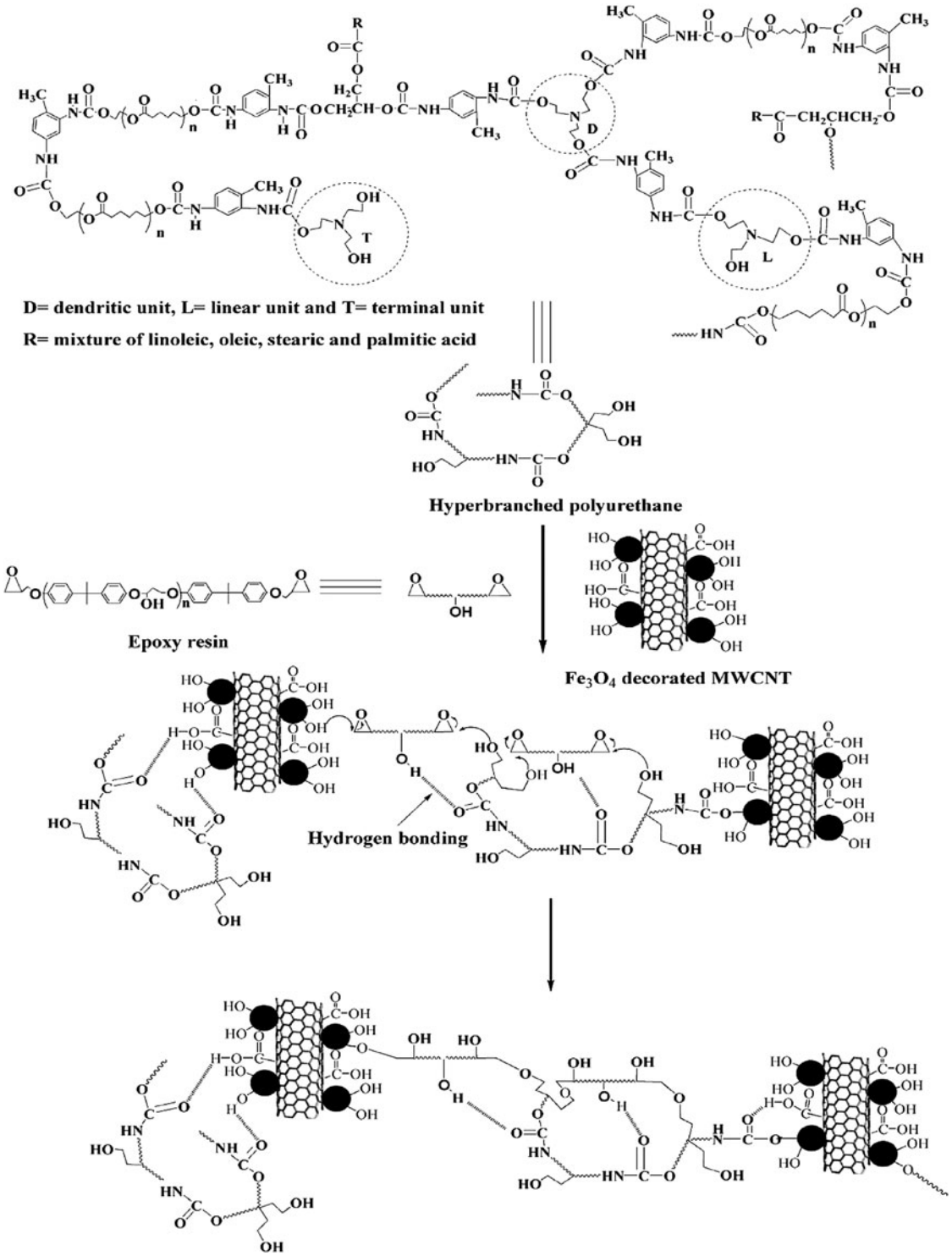
B. Infrared spectroscopic study

The FTIR spectra of the pristine MWCNT, a-MWCNT, Fe_3O_4, and Fe_3O_4-MWCNT are shown in Fig. 1. The absorption band at a frequency of 1725 cm^{-1} [–C=O] was observed in the spectrum of a-MWCNT, whereas such a band was absent for the pristine MWCNT. In the spectrum of Fe_3O_4, the band at 572 cm^{-1} is attributed to the stretching vibration of Fe–O bonds. The band at 3431 cm^{-1} is corresponding to the stretching vibration of Fe–OH groups

TABLE I. Compositions and curing time of the nanocomposites at 120 °C.

Code	HBPU (wt%)	Epoxy (wt%)	Touch free time (min)	Drying time (min)
HBPU	100	...	...	...
HBPU0.2	100	10	51	58
HBPU1	100	10	43	50
HBPU2	100	10	35	43

https://doi.org/10.1557/jmr.2013.213 Published online by Cambridge University Press



SCHEME 1. Proposed cross-linking reactions.

adsorbed on the surface of Fe_3O_4. The absorption bands at 3425 cm^{-1} and at 570 cm^{-1} in the spectrum of Fe_3O_4-MWCNT are the stretching vibration of Fe–OH and Fe–O bonds, respectively. The above results confirmed the presence of Fe_3O_4 in the nanohybrid. Figure 2 presents the FTIR spectra of hyperbranched polyurethane and the nanocomposites. The bands appeared at 3410–3433 cm^{-1} (N–H stretching) and 1726 cm^{-1} (–C=O stretching of urethane linkage) for the urethane groups of pristine polyurethane.[31,32] The bands at 1726 cm^{-1} (–C=O) and at 3410–3433 cm^{-1} (N–H stretching) were found to be shifted to lower wave number (1719–1715 cm^{-1}) and broadened after

https://doi.org/10.1557/jmr.2013.213 Published online by Cambridge University Press

the nanocomposite formation, respectively. The presence of strong interactions between the Fe_3O_4-MWCNT and the polyurethane in the nanocomposites is confirmed from the above results.

C. Raman spectroscopic study

Fig. 3 shows the Raman spectra of the pristine MWCNT, a-MWCNT, and Fe_3O_4-MWCNT. The D and G bands were found at 1342 cm^{-1} and 1572 cm^{-1} for the Raman spectrum of a-MWCNT, respectively. However, the Raman spectrum of Fe_3O_4-MWCNT showed the D and G bands at 1351 cm^{-1} and 1580 cm^{-1}, respectively.[33] The intensity ratio between the D band and the G band (I_D/I_G) implies the degree of defect of the MWCNT. The G band corresponds to the tangential vibration of graphitic carbon atoms, whereas the D band corresponds to the defective graphitic structure. The values of intensity ratios were found to be 0.81, 0.92, and 1.04 for the pristine MWCNT, a-MWCNT, and Fe_3O_4-MWCNT, respectively. The increment of the intensity ratios implies that more defects are generated on the surface of the MWCNT due to the functionalization and adherence of nanoparticles.

D. X-ray diffraction study

The XRD diffractograms of a-MWCNT, Fe_3O_4, and Fe_3O_4-MWCNT are shown in Fig. 4. The XRD diffractogram of Fe_3O_4 showed the peaks at $2\theta = 30.33°$, 35.42°, 56.71°, and 62.72°, which correspond to (220), (311), (511), and (440) planes of Fe_3O_4, respectively.[34] The XRD pattern of a-MWCNT exhibited a peak at $2\theta = 25.41°$ corresponding to the (002) crystal plane of graphite. The XRD diffractogram of Fe_3O_4-MWCNT exhibited the peak at 25.41° corresponding to the (002) crystal plane of graphite along with the peaks of Fe_3O_4. It is confirmed that Fe_3O_4 nanoparticles are attached to the surface of the MWCNT. Figure 5 shows the crystalline structures of hyperbranched polyurethane and the nanocomposites. The diffraction peaks at $2\theta = 20.98°$ and $2\theta = 23.82°$ are due to the (100) and (200) planes of PCL crystals of the hyperbranched polyurethane. The peaks'

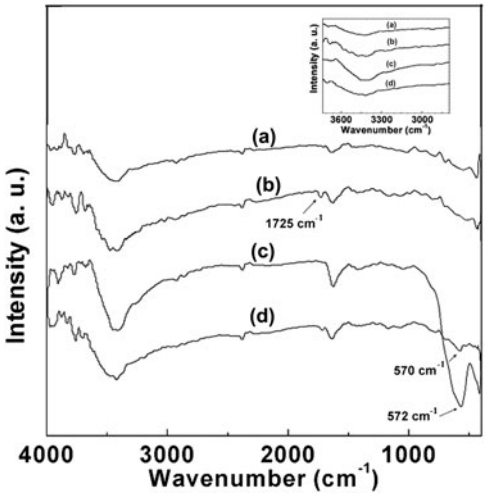


FIG. 1. FTIR spectra with inset of magnified region from 3000 to 3600 cm^{-1} for (a) pristine MWCNT, (b) a-MWCNT, (c) Fe_3O_4, and (d) Fe_3O_4-MWCNT.

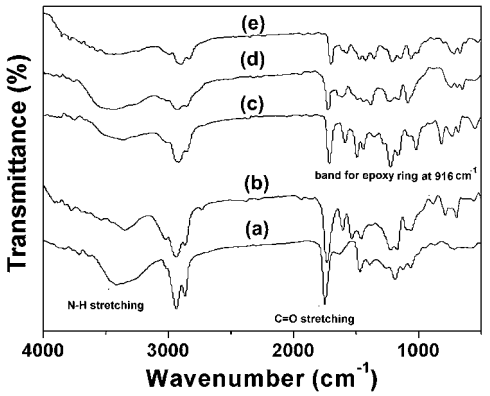


FIG. 2. FTIR spectra for (a) HBPU, (b) HBPU0.2 (before curing), (c) HBPU0.2, (d) HBPU1, and (e) HBPU2.

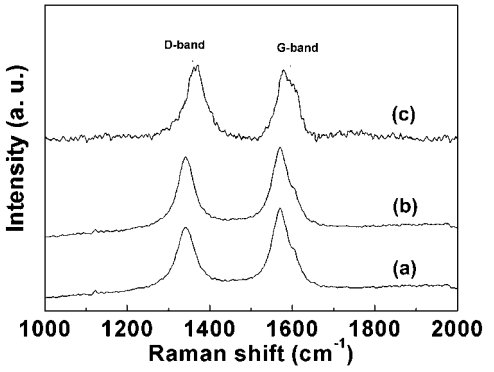


FIG. 3. Raman spectra for (a) pristine MWCNT, (b) a-MWCNT, and (c) Fe_3O_4-MWCNT.

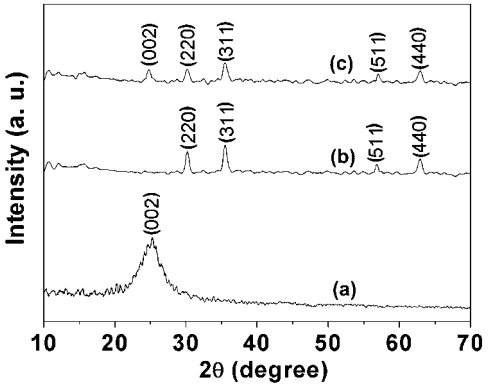


FIG. 4. XRD diffractograms for (a) a-MWCNT, (b) Fe_3O_4, and (c) Fe_3O_4-MWCNT.

https://doi.org/10.1557/jmr.2013.213 Published online by Cambridge University Press

intensity was increased after the nanocomposite formation. This can be attributed to the increased crystallinity for the nucleating effect of the Fe_3O_4-MWCNT in the nanocomposites.[35] The size of the Fe_3O_4 nanoparticles using (220) crystal plane was found to be 9 nm determined by the Scherrer formula.

E. Magnetic property

The magnetic property of the Fe_3O_4-MWCNT and the nanocomposites were studied by the vibrating sample magnetometer at room temperature (Fig. 6). The saturation magnetization values of Fe_3O_4-MWCNT and nanocomposite (HBPU0.2) were found to be 0.23 emu/g and 0.08 emu/g, respectively. The saturation magnetization value of the nanocomposite was lower than that of the Fe_3O_4-MWCNT nanohybrid. This is due to the low content of nanomaterials (0.2 wt%) and surface coating of the Fe_3O_4-MWCNT by the polymer chains in the nanocomposite. The bare MWCNT does not show any magnetic behavior, which indicates that either the amount of remaining catalyst is extremely low or it does not have any magnetic property.

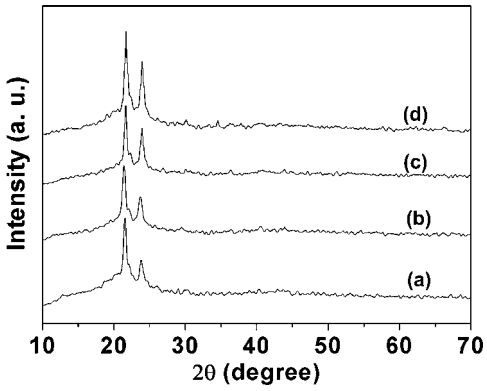


FIG. 5. XRD diffractograms for (a) HBPU, (b) HBPU0.2, (c) HBPU1, and (d) HBPU2.

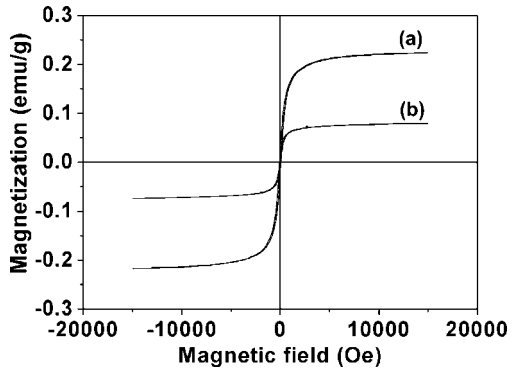


FIG. 6. Magnetic hysteresis loops for (a) Fe_3O_4-MWCNT and (b) HBPU0.2.

F. Morphology study

The morphologies of the a-MWCNT, Fe_3O_4-MWCNT, and the nanocomposite are observed by TEM and shown in Fig. 7. The morphology of a-MWCNT was observed as a smooth surface, whereas that of the Fe_3O_4-MWCNT was rough. From the TEM image, it was observed that Fe_3O_4 nanoparticles are adhered on the surface of the a-MWCNT. The TEM image of the nanocomposite (HBPU1) showed the homogeneous distribution of Fe_3O_4-MWCNT in the polyurethane matrix [Fig. 7(d)]. This is due to the good interaction of Fe_3O_4-MWCNT with the polyurethane matrix. The average size of the Fe_3O_4 nanoparticles was 11 nm. The particle size of the iron oxide was smaller and the saturation magnetization value of the Fe_3O_4-MWCNT was lower as compared to the above-cited literature.[24]

G. Thermal study

The TGA and DTG thermograms of hyperbranched polyurethane and the nanocomposites are shown in Figs. 8(a) and 8(b). The thermal stability was found to be enhanced with the increase of the concentration of Fe_3O_4-MWCNT in the nanocomposites (Table II). This is due to the restricted movement of the polymer chains in the nanocomposites because of various interactions such as H-bonding; polar–polar interaction; and chemical cross-linking among the Fe_3O_4-MWCNT, glycidyl bisphenol-A-based epoxy, and the polyurethane matrix. This can also be attributed to the increased rigidity and compactness of the system due to the increased cross-linking density and supported by the swelling results (Table III). Moreover, the well dispersed highly thermostable Fe_3O_4-MWCNT acts as a gas barrier to the volatile products formed during the decomposition that decreased the permeability and enhanced the thermal stability. The Fe_3O_4-MWCNT-based hyperbranched polyurethane nanocomposites showed enhanced thermal stability as compared to the Fe_3O_4-based nanocomposites.[36]

Figure 9 shows the DSC curves of hyperbranched polyurethane and the nanocomposites. The melting temperature (T_m) and melting enthalpy (ΔH_m) were found to be increased with the increase of the content of Fe_3O_4-MWCNT in the nanocomposites (Table II). This is due to the increased rigidity of the nanocomposites due to the various interactions among the Fe_3O_4-MWCNT, epoxy, and the polyurethane matrix. The degree of crystallinity of all the nanocomposites is given in the Table II. This is determined by the measurement of ΔH_m on cooling and considering an enthalpy value of 136 J/g for 100% crystalline PCL.

H. Mechanical properties

The mechanical properties of the hyperbranched polyurethane and its nanocomposites are given in the Table III. The tensile strength of the nanocomposites increased with the

https://doi.org/10.1557/jmr.2013.213 Published online by Cambridge University Press

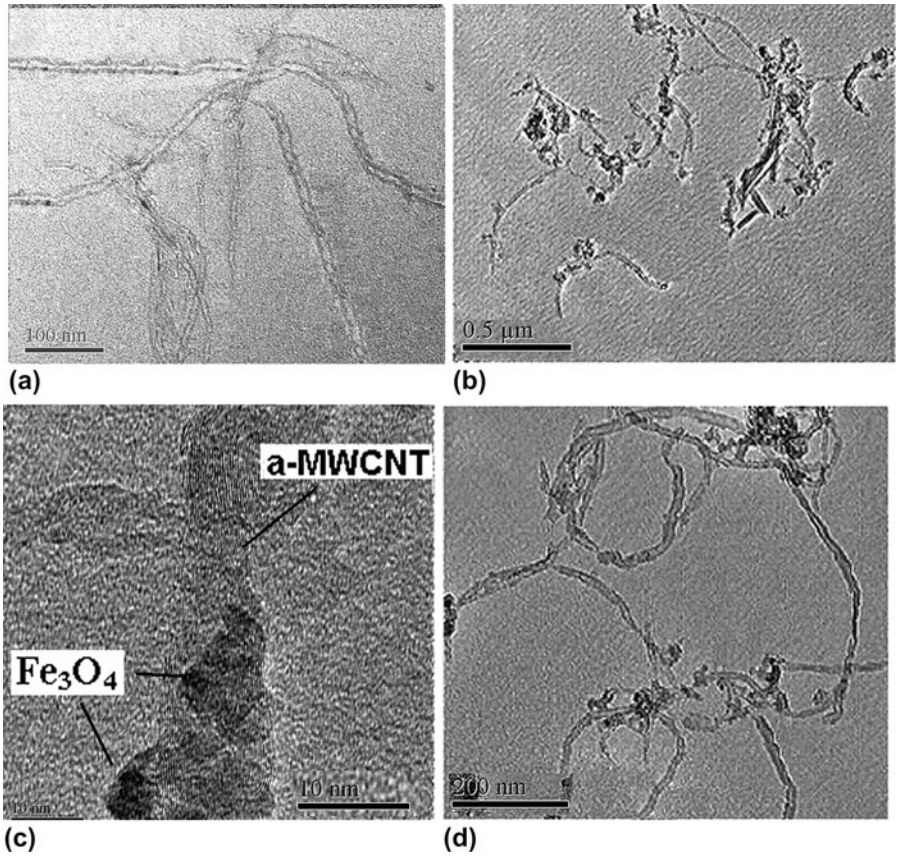


FIG. 7. TEM images for (a) a-MWCNT, (b) and (c) Fe_3O_4-MWCNT, and (d) HBPU1.

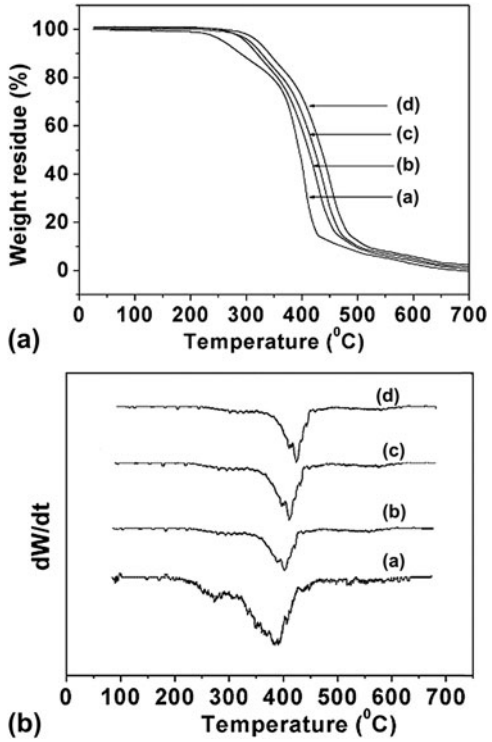


FIG. 8. (a) TGA thermograms for (a) HBPU, (b) HBPU0.2, (c) HBPU1, and (d) HBPU2; and (b) DTG curves for (a) HBPU, (b) HBPU0.2, (c) HBPU1, and (d) HBPU2.

TABLE II. Thermal behaviors of the nanocomposites.

Code	Initial decomposition temperature (°C)	Melting temperature (T_m) °C	Melting enthalpy (ΔH_m J/g)	Degree of crystallinity (%)
HBPU	241	39.5	41	30.14
HBPU0.2	260	40.6	43.1	31.69
HBPU1	274	42.1	44.2	32.5
HBPU2	291	43.2	45.4	33.38

increase of the loading of Fe_3O_4-MWCNT. This is due to the well dispersion of Fe_3O_4-MWCNT and enhanced various interactions among the Fe_3O_4-MWCNT, epoxy, and the polymer matrix.[37–39] As a result, molecular chains are restricted on the surface of the MWCNTs and the chains' slippage decreased during the application of loading. Moreover, this can be attributed to the increased cross-linking density in the system due to the interaction among the epoxide groups, –OH and –COOH of functionalized MWCNT, and free –OH groups of the hyperbranched polyurethane. However, the elongation at break decreases with the increase of the loading of Fe_3O_4-MWCNT in the nanocomposites. This is due to the restricted movement of molecular chains due to the presence of various physico-chemical interactions in the nanocomposites as stated

https://doi.org/10.1557/jmr.2013.213 Published online by Cambridge University Press

TABLE III. Mechanical properties of hyperbranched polyurethane and the nanocomposites.

Property	HBPU	HBPU0.2	HBPU1	HBPU2
Tensile strength (MPa)	6.4 ± 0.4	17 ± 0.3	26.5 ± 0.3	38.5 ± 0.2
Elongation at break (%)	595 ± 3	483 ± 2	434 ± 2	398 ± 2
Scratch hardness (kg)	3.0 ± 0.1	4.6 ± 0.1	6.5 ± 0.1	8.5 ± 0.1
Bending (m)	<0.001	<0.001	<0.001	<0.001
Impact resistance[a] (m)	0.95 ± 0.05	0.95 ± 0.05	0.95 ± 0.05	0.95 ± 0.05
Gloss (60°)	84 ± 2	87 ± 2	91 ± 2	95 ± 2
Swelling (%)	...	29 ± 1.2	22 ± 1.2	16 ± 1.1

[a]1.0 m is the limit of the instrument.

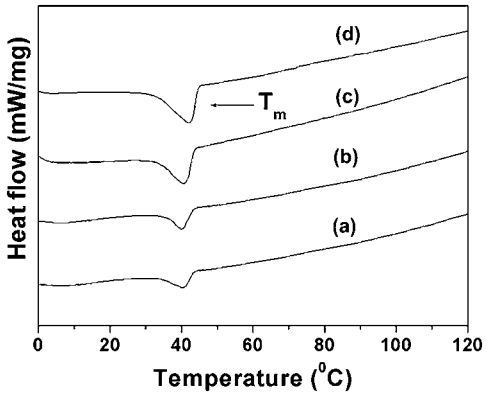


FIG. 9. DSC curves for (a) HBPU, (b) HBPU0.2, (c) HBPU1, and (d) HBPU2.

above. The scratch hardness increased with the increase of the content of Fe_3O_4-MWCNT. The significant improvement of the scratch hardness is due to the increased compactness and rigidity of the nanocomposites. All the prepared nanocomposites exhibited good impact resistance. The Fe_3O_4-MWCNT-based hyperbranched polyurethane nanocomposites exhibited better mechanical properties as compared to the Fe_3O_4-based nanocomposites.[36] The gloss of the nanocomposites increased with the increase of the loading of Fe_3O_4-MWCNT in the nanocomposites. This is attributed to the good compatibility of epoxy resin, Fe_3O_4-MWCNT, and hyperbranched polyurethane and increased the dimension stability of the nanocomposites.

I. Shape memory behaviors

The shape memory behaviors of the hyperbranched polyurethane and the nanocomposites are shown in Fig. 10. The nanocomposites exhibited good shape fixity. The micro-Brownian movements of the polymer chains are frozen and transformed to a rigid state during the cooling. When the polymers are deformed, the orientations of the polymer chains are changed. The free volume or the distance between the polymer chains decreases on stretching, which enhances various interactions such as H-bonding and polar–polar interactions. Thereby it resists the recoiling of the polymer chains and gives the fixed shape. The hyperbranched polyurethane and the nanocomposites exhibited good shape recovery under the microwave stimulus (Table IV). No significant change of shape recovery of the nanocomposites was observed over the repeated cycles (Ten) of test. When the microwave irradiated on the sample, the dipole moment oscillates to align with the external electric field; as a result, heat is generated due to the molecular friction and collisions. The shape recovery effect was observed when the induced heat is close to the transition temperature (T_{trans}). The microwave chamber temperature was found to be 45 °C. The shape recovery time decreased with the increase of the content of Fe_3O_4-MWCNT in the nanocomposites. This can be attributed to the increased stored energy in the nanocomposites due to the homogeneous distribution of the Fe_3O_4-MWCNT and the increased physicochemical cross-link in the systems. CNTs favor to stabilize the crystalline domains of the polymer.[40] They are able to the lock the mechanical constrains. Thus, by increasing the toughness of the polymer, CNTs can allow more energy to be absorbed and restored. Therefore, the strain energy released immediately, when the induced heat is close to the T_{trans}. Furthermore, the increment of shape recovery speed may be due to the enhanced microwave absorption characteristic of the nanohybrid system as both Fe_3O_4 and MWCNT are microwave-absorbing materials.[26,27,41] The increased shape recovery speed may also be due to the enhanced thermal conductivity of the nanocomposites as Fe_3O_4-MWCNT is a conducting material. The nanocomposites showed the almost full recovery in the time period of 42–93 s, so therefore no effect was observed for the longer time of microwave exposure. However, as the exposure time was lesser, the shape recovery was found to be lower. The shape recovery curves of all the samples are shown in Fig. 11. The shape recovery pattern was found to exhibit a sigmoidal shape. The prepared nanocomposites showed the good shape fixity and shape recovery. Hence, the nanocomposites might be utilized as potential SMPs in various fields of applications such as sensors and microactuators, automobile, biomedical devices, and so on.

https://doi.org/10.1557/jmr.2013.213 Published online by Cambridge University Press

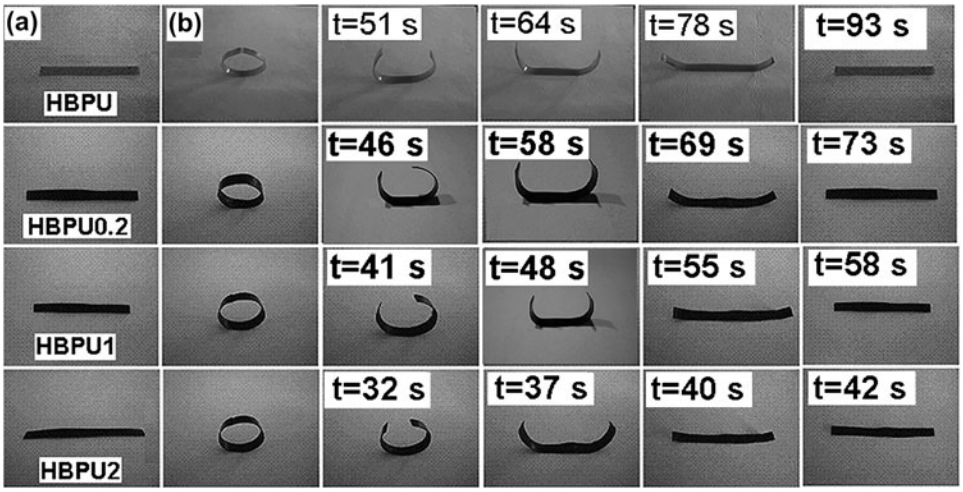


FIG. 10. Shape memory behaviors of hyperbranched polyurethane and the nanocomposites under microwave stimulus (a) original shape and (b) fixed shape.

TABLE IV. Shape memory behaviors of hyperbranched polyurethane and the nanocomposites.

Code	Shape fixity (%)	Shape recovery (%)	Shape recovery time (s)
HBPU	99 ± 0.5	98.5 ± 0.6	93 ± 4
HBPU0.2	99.4 ± 0.2	99.6 ± 0.1	73 ± 2
HBPU1	99.5 ± 0.2	99.6 ± 0.1	58 ± 2
HBPU2	99.5 ± 0.2	99.6 ± 0.1	42 ± 2

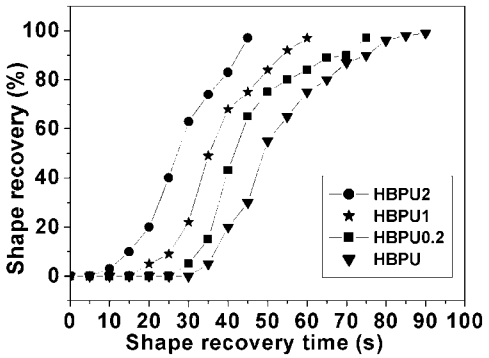


FIG. 11. Shape recovery curves of hyperbranched polyurethane and the nanocomposites.

IV. CONCLUSIONS

From this study, it can be concluded that epoxy modified Fe_3O_4-MWCNT/hyperbranched polyurethane thermosetting nanocomposites exhibited excellent shape recovery under the application of microwave stimulus as well as shape fixity over the repeated cycles of test. The dose-dependent shape memory behavior offers tuning of such property as per the requirement. Significant improvements of tensile strength along with other desired properties including thermal stability were achieved by the nanocomposite synthesis. Thus, the studied nanocomposites have strong potential to be used as noncontact microwave-induced shape memory materials.

ACKNOWLEDGMENTS

The authors express their gratitude and thanks to the research project assistance granted by the Department of Science and Technology (DST), India, through Grant No. SR/S3/ME/0020/2009-SERC, dated 9th July, 2010, SAP (University Grants Commission, UGC), India through Grant No. F.3-30/2009 (SAP-II) and FIST program-2009 (DST), India through the Grant No.SR/FST/CSI-203/209/1 dated 06.05.2010. Mangesh Mahajan is gratefully acknowledged for the magnetic measurement.

REFERENCES

1. W. Small, P. Singhal, T.S. Wilson, and D.J. Maitland: Biomedical applications of thermally activated shape memory polymer. *J. Mater. Chem.* **20**, 3356 (2010).
2. K.M. Lee, H. Koerner, R.A. Vaia, T.J. Bunning, and T.J. White: Light-activated shape memory of glassy, azobenzene liquid crystalline polymer networks. *Soft Matter* **7**, 4318 (2011).
3. C.M. Yakacki: Shape-memory and shape-changing polymers. *Polym. Rev.* **53**, 1 (2013).
4. H.F. Lee, and H.H. Yu: Study of electroactive shape memory polyurethane–carbon nanotube hybrids. *Soft Matter* **7**, 3801 (2011).
5. Y. Cai, J.S. Jiang, B. Zheng, and M.R. Xie: Synthesis and properties of magnetic sensitive shape memory Fe_3O_4/poly(ε-caprolactone)-polyurethane nanocomposites. *J. Appl. Polym. Sci.* **127**, 49 (2013).
6. M. Haghayegh and G.M.M. Sadeghi: Synthesis of shape memory polyurethane/clay nanocomposites and analysis of shape memory, thermal, and mechanical properties. *Polym. Compos.* **33**, 843 (2012).
7. M.K. Jang, A. Hartwig, and B.K. Kim: Shape memory polyurethanes cross-linked by surface modified silica particles. *J. Mater. Chem.* **19**, 1166 (2009).

https://doi.org/10.1557/jmr.2013.213 Published online by Cambridge University Press

8. I.A. Rousseau: Challenges of shape memory polymers: A review of the progress toward overcoming SMP's limitations. *Polym. Eng. Sci.* **48**, 2075 (2008).
9. J.M. Cuevas, R. Rubio, J.M. Laza, J.L. Vilas, M. Rodriguez, and L.M. Leon: Shape memory composites based on glass-fibre-reinforced poly(ethylene)-like polymers. *Smart Mater. Struct.* **21**, 035004 (2012).
10. J. Xu, W. Shi, and W. Pang: Synthesis and shape memory effects of Si–O–Si cross-linked hybrid polyurethanes. *Polymer* **47**, 457 (2006).
11. C.S. Zhang and Q.Q. Ni: Bending behavior of shape memory polymer based laminates *Compos. Struct.* **78**, 153 (2007).
12. H. Deka and N. Karak: Shape-memory property and characterization of epoxy resin-modified Mesua ferrea L. seed oil-based hyperbranched polyurethane. *J. Appl. Polym. Sci.* **116**, 106 (2010).
13. R. Rajasekaran and M. Alagar: Mechanical properties of bismaleimides modified polysulfone epoxy matrices. *Int. J. Polym. Mater.* **56**, 911 (2007).
14. K.P. Unnikrishnan and E.T. Thachil: Toughening of epoxy resins. *Des. Monomers Polym.* **9**, 129 (2006).
15. M. Hemmati, A. Narimani, H. Shariatpanahi, A. Fereidoon, and M.G. Ahangari: Study on morphology, rheology and mechanical properties of thermoplastic elastomer polyolefin (TPO)/carbon nanotube nanocomposites with reference to the effect of polypropylene-grafted-maleic anhydride (PP-g-MA) as a compatibilizer. *Int. J. Polym. Mater.* **60**, 384 (2011).
16. M. Rahmat and P. Hubert: Carbon nanotube–polymer interactions in nanocomposites: A review. *Compos. Sci. Technol.* **72**, 72 (2011).
17. Y.T. Wang, C.S. Wang, H.Y. Yin, L.L. Wang, H.F. Xie, and R.S. Cheng: Carboxyl-terminated butadiene-acrylonitrile-toughened epoxy/carboxyl-modified carbon nanotube nanocomposites: Thermal and mechanical properties. *Express Polym. Lett.* **6**, 719 (2012).
18. J.C. Zhao, F.P. Du, X.P. Zhou, W. Cui, X.M. Wang, H. Zhu, X.L. Xie, and Y.W. Mei: Thermal conductive and electrical properties of polyurethane/hyperbranched poly(urea-urethane)-grafted multi-walled carbon nanotube composites. *Composites Part B* **42**, 2111 (2011).
19. S. Taheri, E. Nakhlband, and H. Nazockdast: Microstructure and multiwall carbon nanotube partitioning in polycarbonate/acrylonitrile-butadiene-styrene/multiwall carbon nanotube nanocomposites. *Polym. Plast. Technol. Eng.* **52**, 300 (2013).
20. N.G. Sahoo, S. Rana, J.W. Cho, L. Li, and S.H. Chan: Polymer nanocomposites based on functionalized carbon nanotubes. *Prog. Polym. Sci.* **35**, 837 (2010).
21. P. Song, Y. Shen, B. Du, Z. Guo, and Z. Fang: Fabrication of fullerene-decorated carbon nanotubes and their application in flame-retarding polypropylene. *Nanoscale* **1**, 118 (2009).
22. J. Khanderi, R.C. Hoffmann, A. Gurlo, and J.J. Schneider: Synthesis and sensoric response of ZnO decorated carbon nanotubes. *J. Mater. Chem.* **19**, 5039 (2009).
23. Q. Zhang, M. Zhu, Q. Zhang, Y. Li, and H. Wang: The formation of magnetite nanoparticles on the sidewalls of multi-walled carbon nanotubes. *Compos. Sci. Technol.* **69**, 633 (2009).
24. L. Kong, X. Lu, and W. Zhang: Facile synthesis of multifunctional multiwalled carbon nanotubes/Fe_3O_4 nanoparticles/polyaniline composite nanotubes. *J. Solid State Chem.* **181**, 628 (2008).
25. H.Y. Li, C.M. Chang, K.Y. Hsu, and Y.L. Liu: Poly(lactide)-functionalized and Fe_3O_4 nanoparticle-decorated multiwalled carbon nanotubes for preparation of electrically-conductive and magnetic poly(lactide) films and electrospun nanofibers. *J. Mater. Chem.* **22**, 4855 (2012).
26. Y. Zhan, R. Zhao, Y. Lei, F. Meng, J. Zhong, and X. Liu: A novel carbon nanotubes/Fe_3O_4 inorganic hybrid material: Synthesis, characterization and microwave electromagnetic properties. *J. Magn. Magn. Mater.* **323**, 1006 (2011).
27. S. Ni, S. Lin, Q. Pan, F. Yang, K. Huang, and D. He: Hydrothermal synthesis and microwave absorption properties of Fe_3O_4 nanocrystals. *J. Phys. D: Appl. Phys.* **42**, 055004 (2009).
28. S. Dutta and N. Karak: Effect of the NCO/OH ratio on the properties of *Mesua Ferrea L.* seed oil-modified polyurethane resins. *Polym. Int.* **55**, 49 (2006).
29. H. Kalita and N. Karak: *Mesua ferrea* L. seed oil-based hyperbranched shape memory polyurethanes: Effect of multifunctional component. *Polym. Eng. Sci.* **52**, 2454 (2012).
30. Y.C. Jung, H.H. So, and J.W. Cho: Water-responsive shape memory polyurethane block copolymer modified with polyhedral oligomeric silsesquioxane. *J. Macromol. Sci. Phys.* **45**, 453 (2006).
31. Y. Zhang, R.J. Heath, and D.J. Hourston: Morphology, mechanical properties, and thermal stability of polyurethane–epoxide resin interpenetrating polymer network rigid foams. *J. Appl. Polym. Sci.* **75**, 406 (2000).
32. S.D. Desai, A.L. Emanuel, and V.K. Sinha: Polyester polyol-based polyurethane adhesive; effect of treatment on rubber surface. *J. Polym. Res.* **10**, 141 (2003).
33. S. Thakur and N. Karak: Green reduction of graphene oxide by aqueous phytoextracts. *Carbon* **50**, 5331 (2012).
34. J.O. Park, K.Y. Rhee, and S.J. Park: Silane treatment of Fe_3O_4 and its effect on the magnetic and wear properties of Fe_3O_4/epoxy nanocomposites. *Appl. Surf. Sci.* **256**, 6945 (2010).
35. H. Deka, N. Karak, R.D. Kalita, and A.K. Buragohain: Biocompatible hyperbranched polyurethane/multi-walled carbon nanotube composites as shape memory materials. *Carbon* **48**, 2013 (2010).
36. H. Kalita and N. Karak: Bio-based hyperbranched polyurethane/Fe_3O_4 nanocomposites as shape memory materials. *Polym. Adv. Technol.* doi: 10.1002/pat.3149.
37. S. Rana, N. Karak, J.W. Cho, and Y.H. Kim: Enhanced dispersion of carbon nanotubes in hyperbranched polyurethane and properties of nanocomposites. *Nanotechnology* **19**, 495707 (2008).
38. S.K. Yadav, S.S. Mahapatra, and J.W. Cho: Synthesis of mechanically robust antimicrobial nanocomposites by click coupling of hyperbranched polyurethane and carbon nanotubes. *Polymer* **53**, 2023 (2012).
39. S.S. Mahapatra, S.K. Yadav, H.J. Yoo, J.W. Cho, and J.S. Park: Highly branched polyurethane: Synthesis, characterization and effects of branching on dispersion of carbon nanotubes. *Composites Part B* **45**, 165 (2013).
40. L. Viry, C. Mercader, P. Miaudet, C. Zakri, A. Derre, A. Kuhn, M. Maugey, and P. Poulin: Nanotube fibers for electromechanical and shape memory actuators. *J. Mater. Chem.* **20**, 3487 (2010).
41. W. Zhou, X. Hu, X. Bai, S. Zhou, C. Sun, J. Yan, and P. Chen: Synthesis and electromagnetic, microwave absorbing properties of core–shell Fe_3O_4–poly(3, 4-ethylenedioxythiophene) microspheres. *ACS Appl. Mater. Interfaces* **3**, 3839 (2011).

https://doi.org/10.1557/jmr.2013.213 Published online by Cambridge University Press